5. RESULTS

5.1 Results for Ru/SiO_2 Catalysts

5.1.1 Preliminary Experimentation

The mass spectra for several standard gas samples were gathered so that the cracking patterns in the spectrometer of the species expected to be formed during reaction could be accurately determined. In addition, knowledge of the ionization characteristics of the spectrometer is necessary for identification of unknown species. Scans of CO, CH_4, C_2H_4 and C_2H_6 standard samples are shown in the Appendix. It was found that an emission current of 0.58 mA prevented excessive fragmentation of most of these species while retaining sufficient sensitivity. These spectra are quite similar to those compiled in the literature [106], and so it is expected that the appearance of any unknown species during experimentation can be identified through comparison with tabulated spectra.

Next, the room-temperature CO-deposition process onto the Ru/SiO_2 catalyst was monitored to examine the mechanism of carbon deposition. One atmosphere of CO was exposed to the catalyst while monitoring the gas over the catalyst to detect the presence or absence of CO_2 formation from disproportionation of CO; no CO_2 formation was detected. Also, since the experimental procedure used in this study required heating the catalyst sample to reaction temperatures (while under vacuum) after adsorption of CO at room temperature, the desorption characteristics of CO were examined to assure that no CO desorbed from the surface of the catalyst during this heating period. At the reaction temperatures used, from 400 K to 525 K, no CO desorption was observed during heating from 300 K, which typically

required less than ten minutes. In addition, to avoid catalyst deactivation, care was taken that the temperature of the catalyst at no time exceeded 675 K, as carbon deposition as graphite is reported to occur at 700 K [14].

5.1.2 Methanation Reactions

Scans of the mass spectra taken at several points during reaction reveal that, upon exposure to 460 torr of hydrogen, product species were formed with major mass peaks at $m/e^- = 15$, 16, 18 and 28 (Figure 3). These peaks were assigned through comparison with standard mass spectra tables as follows: 15 - CH_3, 16 - CH_4 and O, 18 - H_2O and 28 - CO. Accordingly, when monitoring methane, the mass at 15 was used to avoid interference with atomic oxygen at 16, formed from fragmentation of H_2O and CO. In addition, $m/e^- = 2$ was monitored to observe the response of hydrogen admission to the reaction cell, as well as $m/e^- = 28$ and 44 to monitor possible CO desorption and CO_2 formation, respectively.

Figure 4 shows a typical reaction experiment at 423 K where the catalyst sample is exposed to hydrogen at time zero; figures for other temperatures are given in the Appendix. The hydrogen partial pressure is large enough to be considered constant with respect to the other species which form and desorb during reaction. Therefore, all mass signals are normalized with respect to the hydrogen signal. As can be seen, methane begins to form immediately, and within 30 to 40 seconds, a linear trend is evident in its formation. The signals for CO and CO_2 did not change significantly during the course of the experiment, evidence that neither hydrogen-assisted CO desorption nor the water-gas shift reaction occurred appreciably under these conditions. Also shown in this figure is the linear

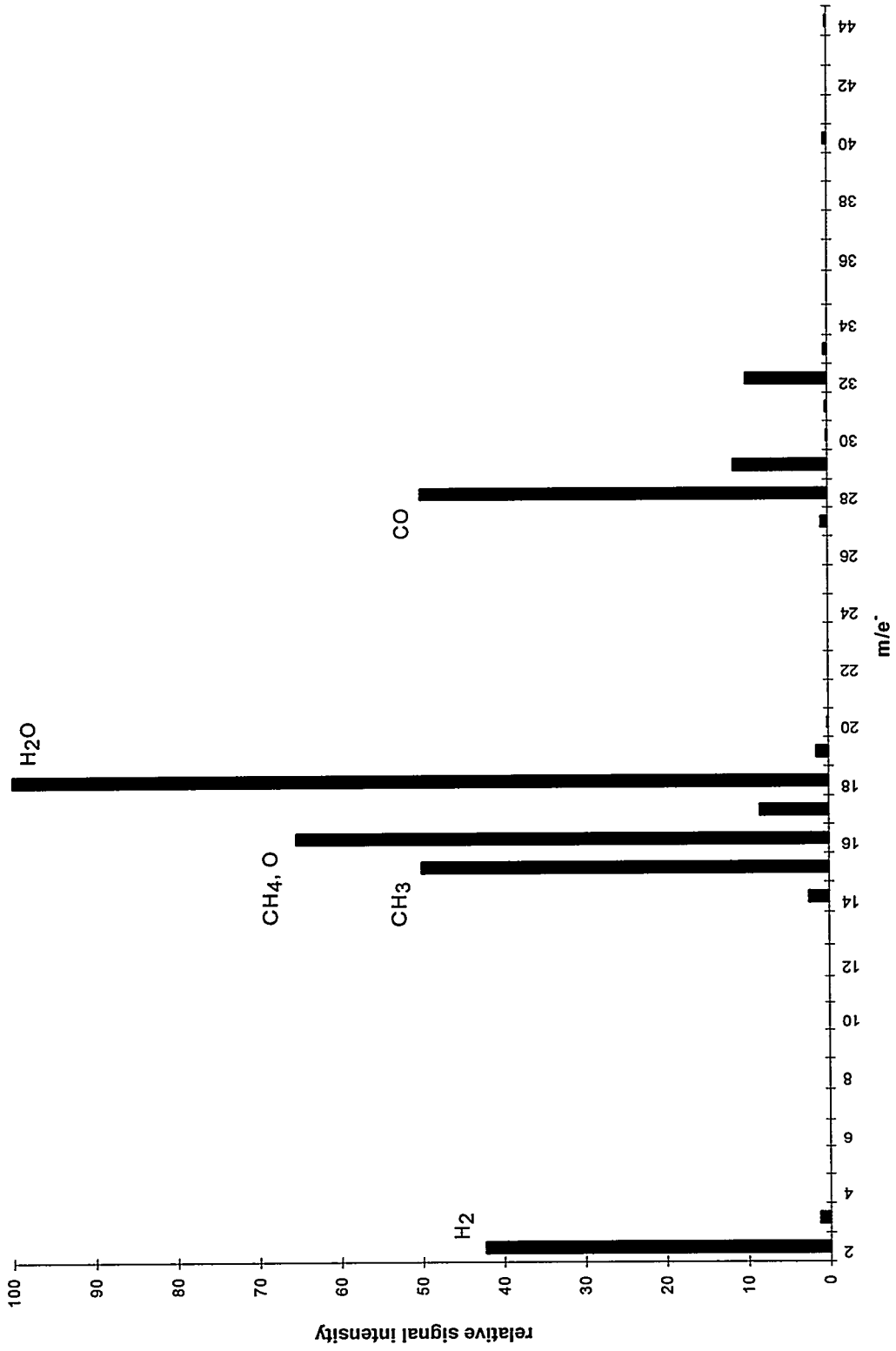

FIGURE 3. Product mixture spectra (473 K, 460 torr)

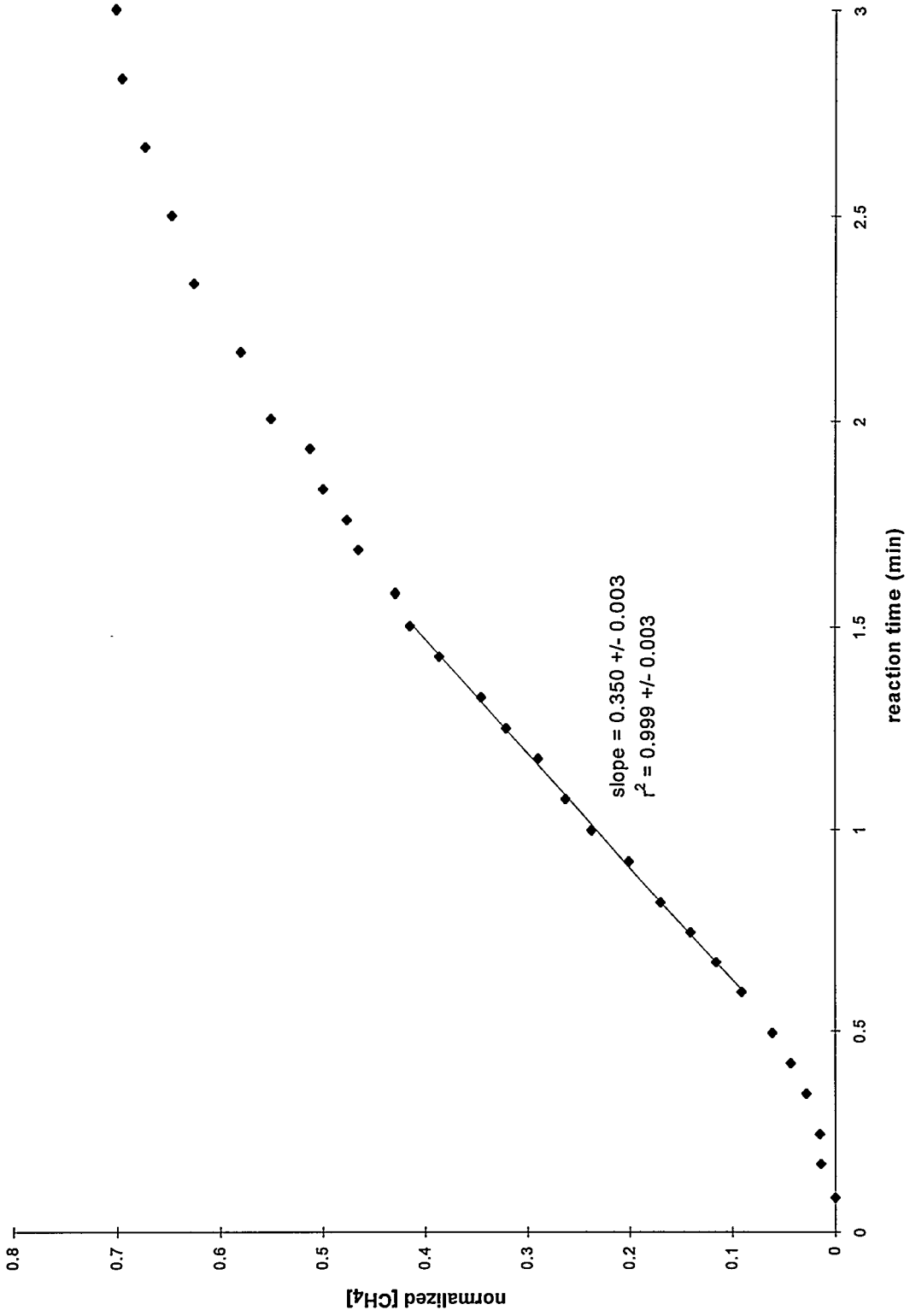

FIGURE 4. Methane formation over 4% Ru/SiO_2 (423 K, 460 torr)

regression of the steady-state portion of the data used to calculate the initial rate of methane formation. Table 2 summarizes the TOF's resulting from the regression of the raw data for each experiment. The statistical regression values used to calculate these rates, and the standard errors in these values, are given in the Appendix.

5.1.3 Kinetic Parameters

The turnover frequencies, expressed as moles of CH_4 per mol Ru surface atom per second, for temperatures from 400 K to 474 K from Table 2 are plotted in Figure 5. The TOF varies from around 0.0001 to 0.01 over this temperature range. As can be seen, a nearly linear trend is apparent for a lower temperature range, with negative deviations from this trend above 450 K. The reasons for this deviation are discussed later. Accordingly, only the data for the three lowest temperatures were used in the kinetic analysis of the Ru/SiO_2

TABLE 2. Summary of kinetic parameters for CO hydrogenation over Ru/SiO_2

temperature (K)	**TOF (10^{-3} mol CH_4 /mol Ru_s /sec)**
400	0.0949
400	0.157
401	0.217
402	0.0959
420	0.456
421	0.796
421	0.649
423	0.772
440	1.88
443	2.74
443	1.90
443	1.76
473	5.75
473	6.12
474	4.27

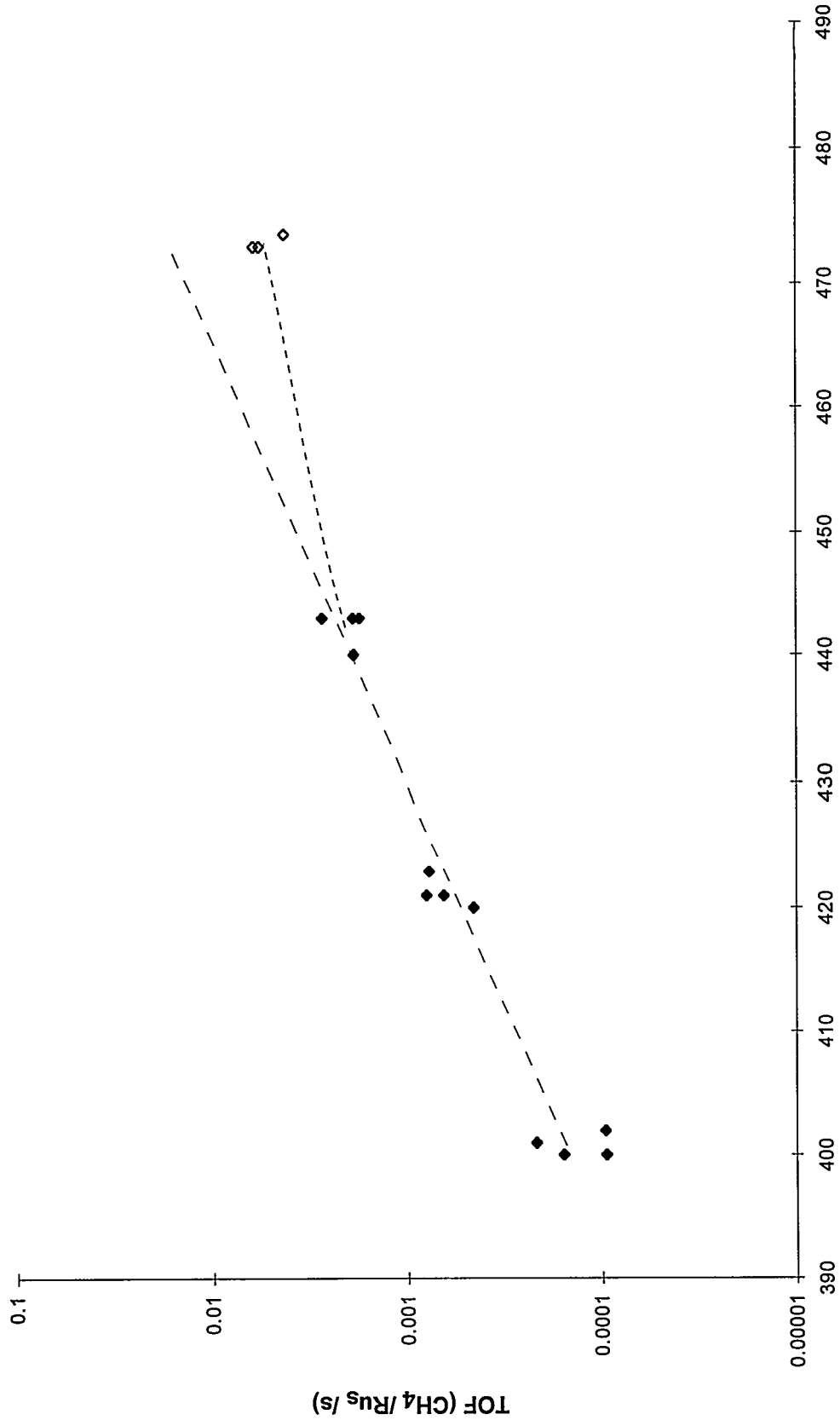

FIGURE 5. Turnover frequencies for methane formation over 4% Ru/SiO_2

catalyst.

Figure 6 shows the Arrhenius plot along with the results of a linear regression of the lower temperature data. The slope of this line yields an apparent activation energy of 23.2 kcal/mol, with the linear regression yielding a standard error of ± 1.7 kcal/mol.

5.1.4 ^{1}H-NMR Experimentation

Next, the results from these studies were correlated with those for an identical ^{1}H-NMR study conducted at 400 K, the same temperature at which previous H_2 microcalorimetry studies were conducted (higher temperature data will be presented in [107]). During the course of the reaction, two H/Ru resonances, corresponding to weakly adsorbed hydrogen, were monitored as the reaction progressed. Figure 7 shows the development of these resonance peaks, at approximately -45 ppm and -55 ppm, upon exposure of the CO-saturated catalyst to 460 torr of H_2. The center resonance peak is due to hydroxyl groups on the silica support.

Figure 8 shows the resulting total H/Ru_s (adsorbed hydrogen per surface ruthenium atom) as a function of time during reaction at 400 K. As can be seen from this figure, upon exposure of the CO-saturated catalyst to 460 torr of hydrogen gas, the H/Ru_s signal rises rapidly at first to a value of about 1, after which adsorption occurs more slowly. After an exposure time of 90 minutes, the coverage approaches an asymptotic value of about 2.5 H/Ru_s.

Figure 9 shows the correlation between the reaction rate and hydrogen adsorption, where the time dimension has been removed to correlate the rate of methane formation as a function of hydrogen coverage. As this figure shows, the rate increases rapidly to a value of

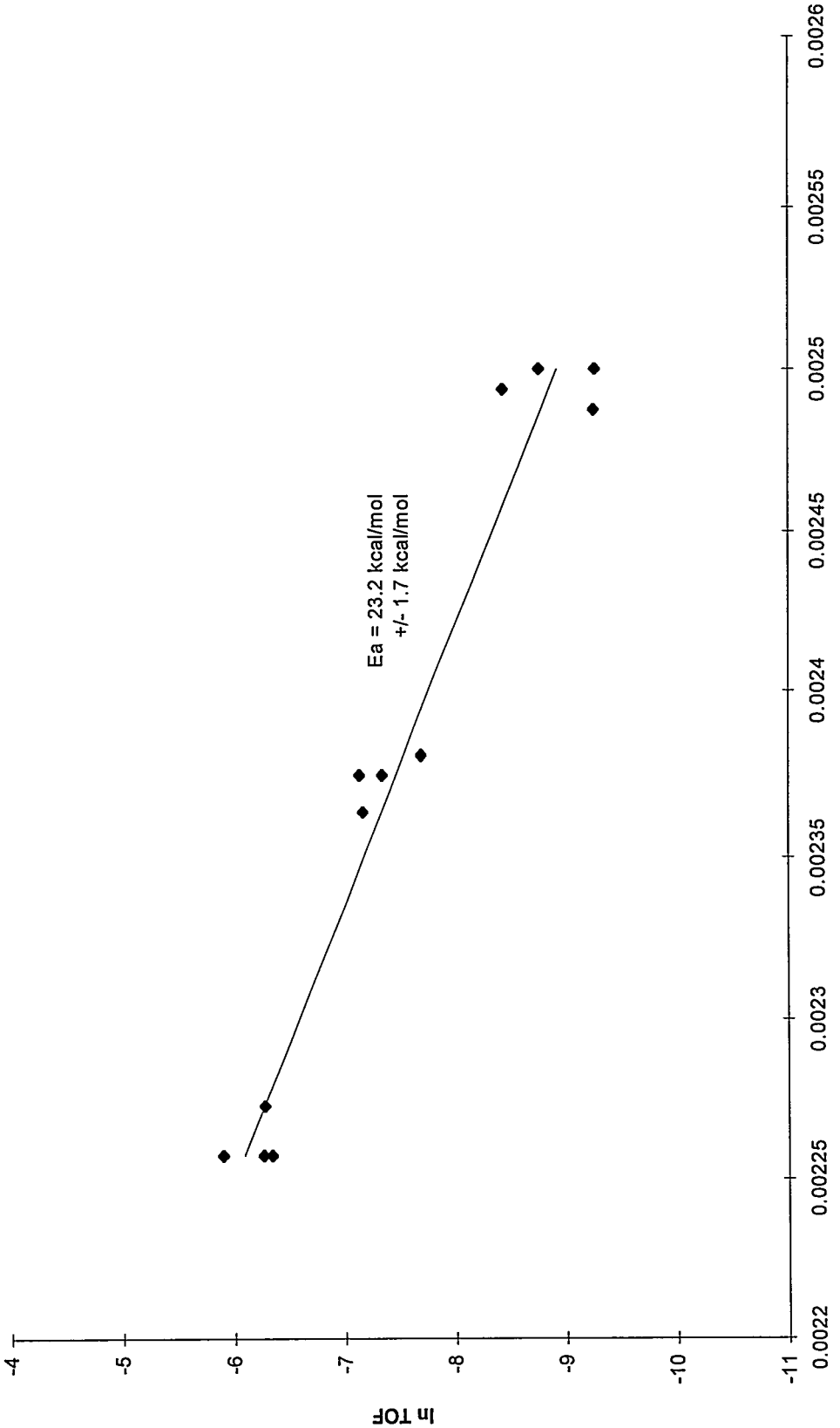

FIGURE 6. Arrhenius plot for methane formation over 4% Ru/SiO_2

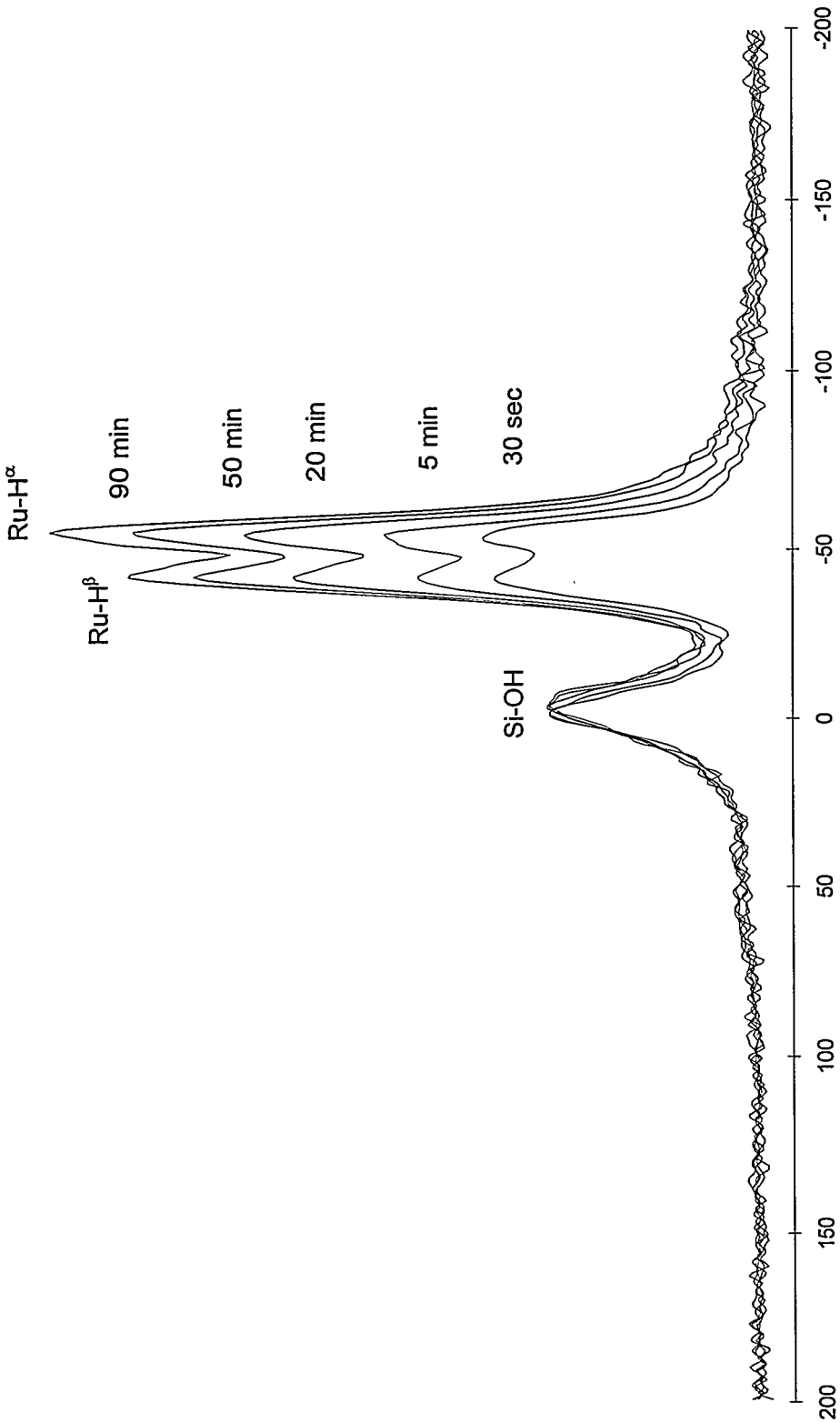

FIGURE 7. Hydrogen adsorption on 4% Ru/SiO_2 during CO hydrogenation (400 K, 460 torr)

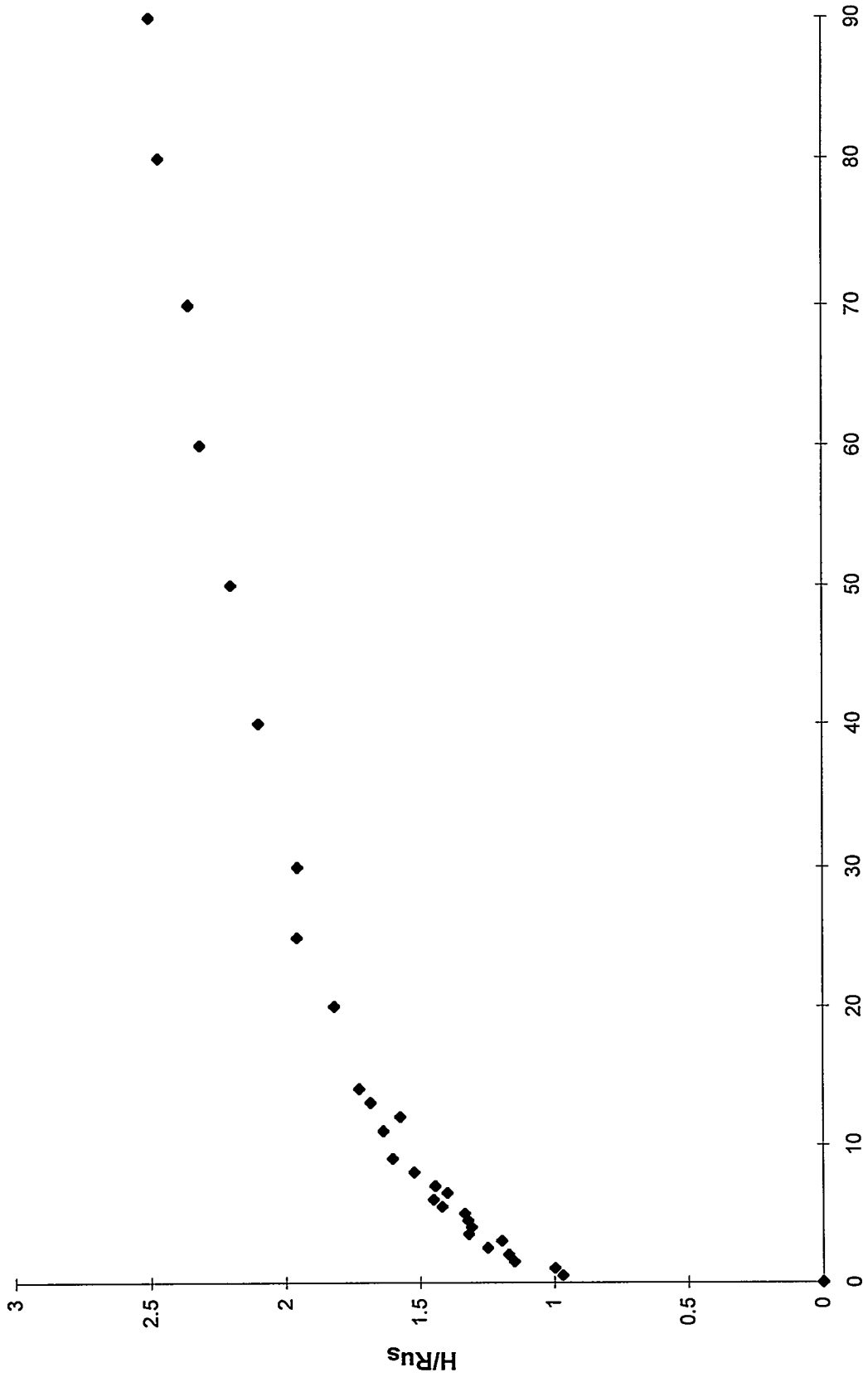

Figure 8. Hydrogen coverage during methanation over Ru/SiO_2 (400 K, 460 torr)

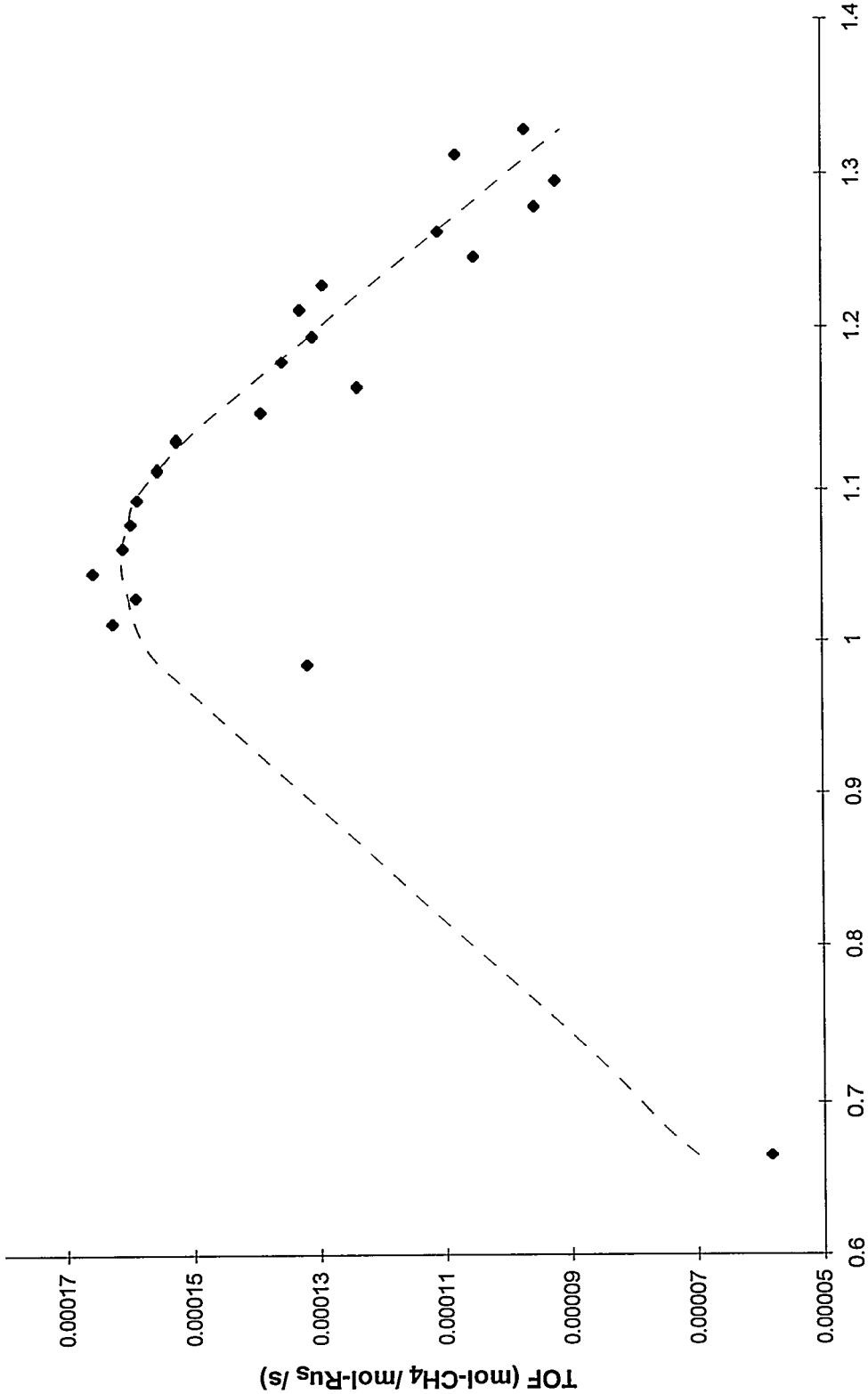

FIGURE 9. Change in methanation rate with hydrogen coverage over Ru/SiO_2 (400 K, 460 torr)

about 1 H/Ru_s, and then remains relatively constant for a short period of time until a value of approximately 1.1, after which the rate of methane formation decreases rapidly.

5.2 Results for Ag-Ru/SiO_2 Catalysts

Experiments were repeated for a series of Ag-Ru/SiO_2 bimetallic catalysts with silver contents of 3, 10, 20 and 30 atomic percent (of total metal content). Table 3 summarizes the kinetic parameters for these catalysts. See the Appendix for graphic representation of the data from which these parameters were calculated. Note that in some of these figures, lower temperature data is omitted for clarity. Figure 10 shows the dramatic effect the addition of silver has on the formation of methane. As little as 3% Ag causes the formation of methane to slow significantly, with additional Ag having a less pronounced effect. In addition, as discussed below, the temperature dependence of this rate was also shown to decrease.

5.2.1 Methanation Reactions

The decrease in the rate of methane formation is present at all temperatures studied, as shown in Figure 11, where the monometallic data is included for comparison. The TOF's for the 3% and 10% Ag catalysts showed little difference from one another, but were both about 80% lower than in the monometallic case. Further addition of 20 to 30% Ag resulted in rates that were about 95% lower than the monometallic catalyst.

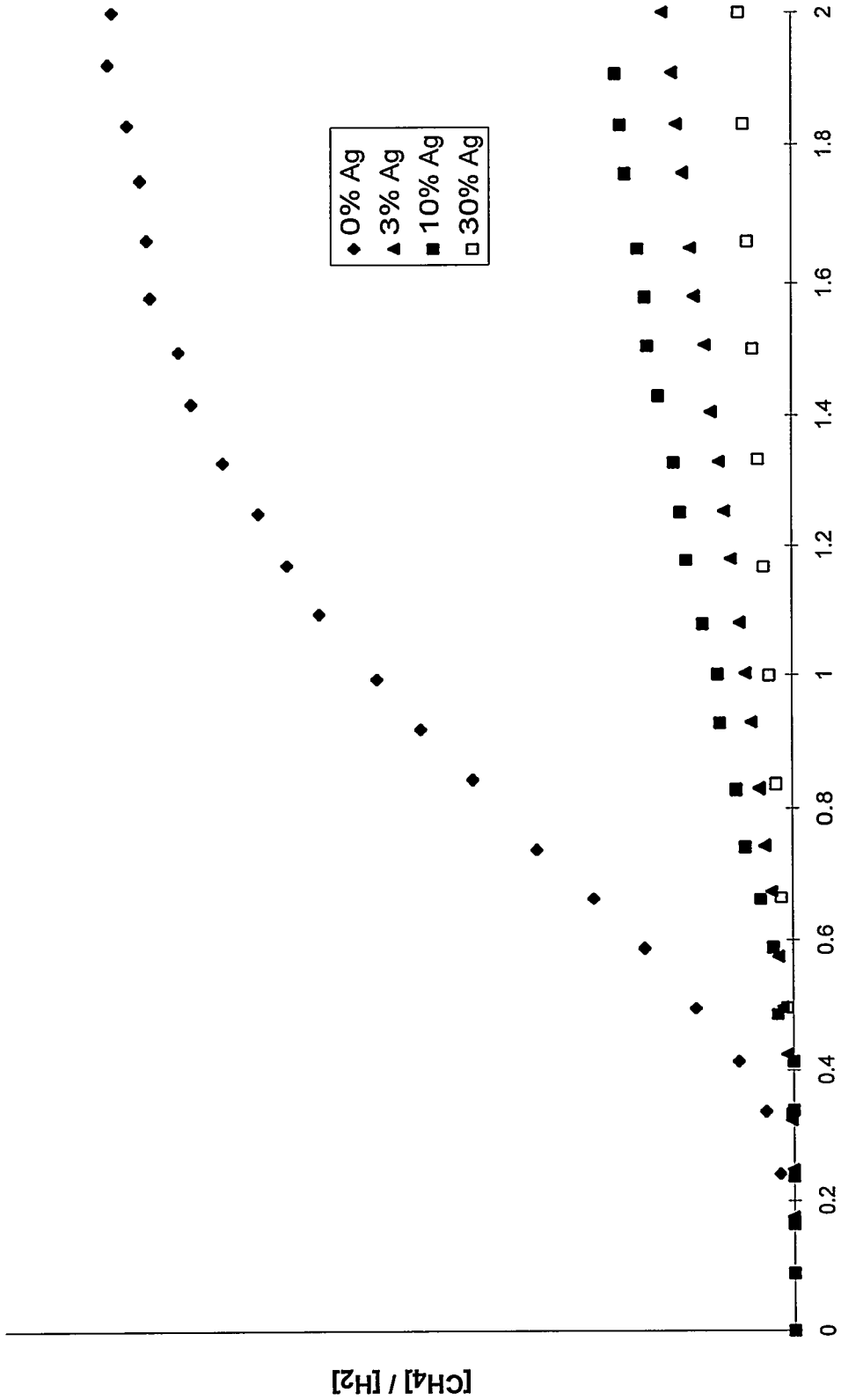

FIGURE 10. Effect of silver addition on methane formation over Ru/SiO_2 (443 K, 460 torr)

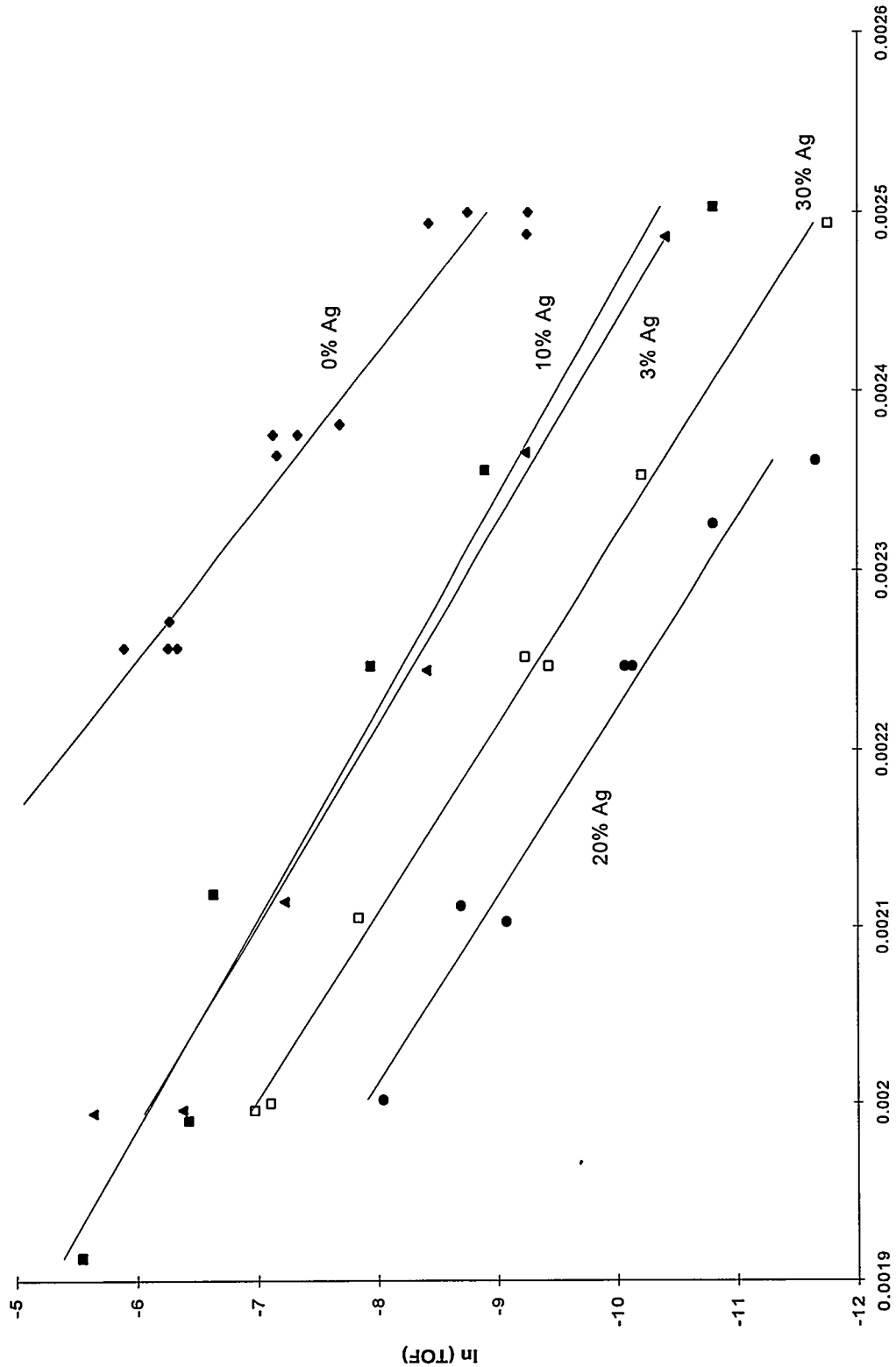

FIGURE 11. Arrhenius plot for methane formation over Ag-Ru/SiO_2

5.2.2 Kinetic Parameters

Figure 12 shows the effect of Ag addition on the apparent activation energy for methane formation. From this figure, it is apparent that the net effect is to lower the activation energy from its initial value of about 23 kcal/mol to about 18 kcal/mol. The activation energies for 3, 10, 20 and 30% Ag are all approximately constant within experimental error. As this figure shows, the effect is complete at silver contents as low as

TABLE 3. Summary of kinetic parameters for CO hydrogenation over Ag-Ru/SiO_2

catalyst	**temperature**	**TOF (10^{-3} mol CH_4 /mol Ru_s /sec)**
3% Ag-Ru/SiO_2	402	0.0302
	423	0.0973
	446	0.222
	473	0.727
	501	1.697
	502	3.553
10% Ag-Ru/SiO_2	400	0.0203
	425	0.136
	445	0.354
	472	1.31
	503	1.61
	523	3.91
20% Ag-Ru/SiO_2	424	0.00867
	430	0.0203
	445	0.0424
	445	0.0397
	474	0.167
	476	0.114
	500	0.321
30% Ag-Ru/SiO_2	401	0.00785
	425	0.0368
	444	0.0975
	445	0.0801
	475	0.393
	501	0.934
	500	0.818

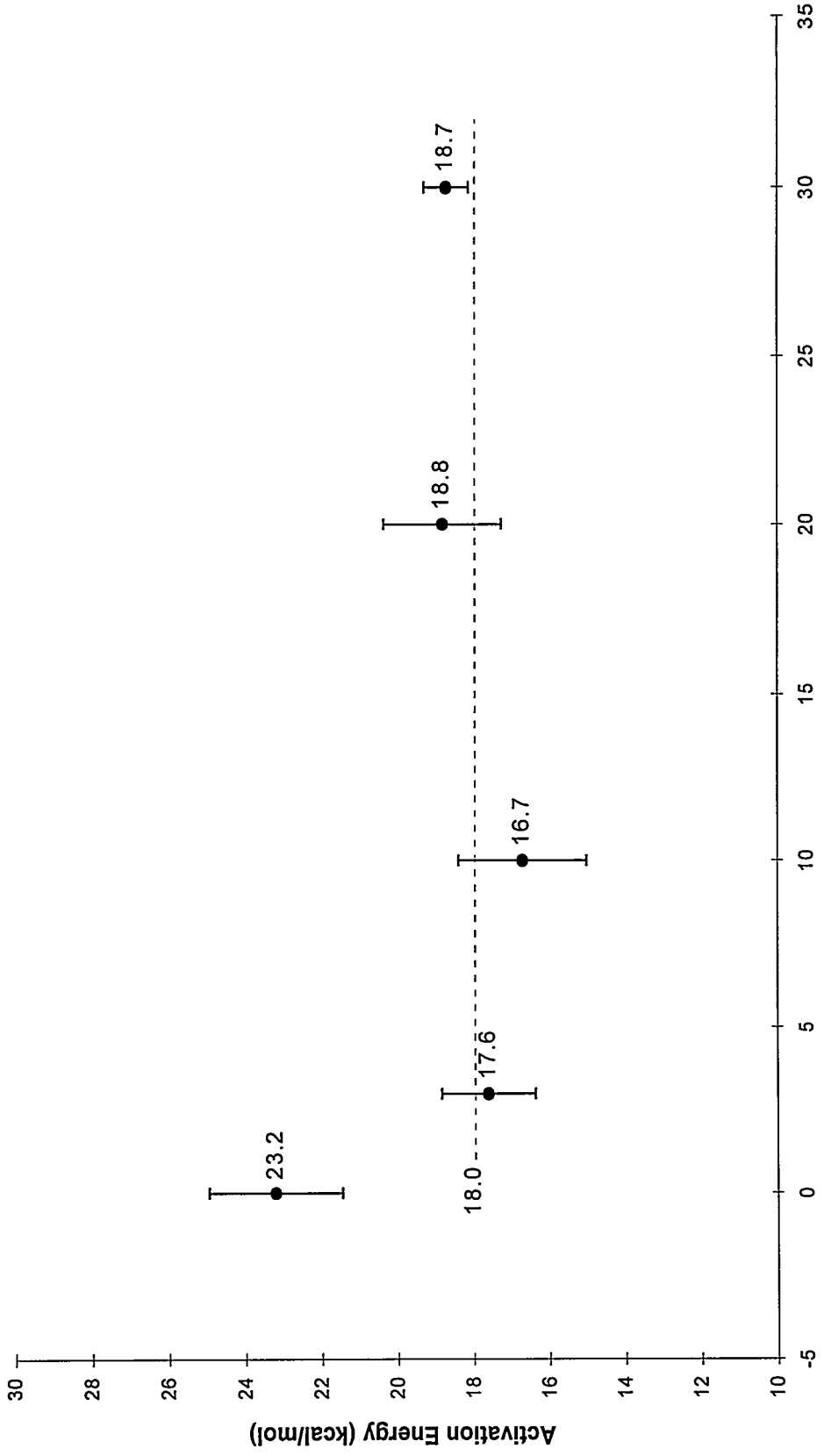

FIGURE 12. Effect of silver addition on apparent activation energy

3%, and no significant change in the activation energy occurs upon further Ag addition. The error bars in this figure represent the standard deviation in the activation energy obtained from a linear regression of the experimental data in Table 2 and Table 3.